Numerical and Experimental Assessment of the Performance of Four Nondestructive Damage Evaluation Methods in Situations Comparable to Post-Earthquake Damage Analysis.

Philippe Guéguen*, Alaa Hamze*,Laurent Baillet*, Philippe Roux*

*ISTerre, CNRS/IFSTTAR, Grenoble Alpes university, BP 53, 38041 Grenoble cedex9, France,
Corresponding Author: Philippe Guéguen - philippe.gueguen@ujf-grenoble.fr

SUMMARY – This study evaluates several methods for the detection and location of a perturbation along a bending beam. Unlike previous studies, the situation chosen is comparable to that encountered in-situ after an earthquake. Indeed, assessment of earthquake damage to buildings is a crucial factor in crisis management. Buildings can be tested appropriately using operational modal analysis methods based on ambient vibration data. In this study, we tested four modal-based methods to locate the perturbation. The mode shapes and eigenfrequencies of a beam were evaluated in the laboratory using the frequency domain decomposition method applied to ambient vibrations simulated along a one-dimensional bending beam, using the finite element method and recorded on a poly(methyl methacrylate) (Plexiglas) beam-like free-clamped structure. The data show that the uniform load surface curvature method is the most efficient, and it allows for accurate estimation of the location of the perturbation, whatever its nature (e.g., multiple, simple, different positions). The experimental data also show that frequency domain decomposition resolution of the mode shapes must be as accurate as possible, otherwise it is impossible to locate transient perturbations over short periods.

Key words: damage, location, mode-based methods, experiment, numerical

1. Introduction

Over the last two decades, a significant amount of research has been conducted on nondestructive damage evaluation (NDE) through the monitoring of changes in the dynamic modal response of structures. NDE is a critical issue with extreme events such as earthquakes, during which fast and accurate estimation of building damage is essential to seismic crisis management. Rytter [1993] classified the NDE methods into four levels according to their objectives: level I, detection of damage; level II, identification of damage location; level III, quantification of damage severity; and level IV, prognosis for the remaining life-time of the structure.

The first level corresponds to the detection of any changes that occur during an earthquake. Analysis of damage related to variations in the modal parameters of buildings is common practice in earthquake engineering. Salawu [1997] discussed the drawbacks of the use of natural frequencies as diagnostic parameters, due to their sensitivity to external loading, such as air temperature. However, Farrar and Worden [2007] reported that frequencies are certainly the most sensitive modal parameters to changes, particularly because the loss of stiffness has a direct impact on the frequencies of the building. In addition, resonant frequencies show much less statistical variation from random error sources than other modal parameters [Doebling et al., 1997]. In most cases, structural damage detection after earthquakes is based on comparing the 'ante-damage' state and the 'post-damage' state [Régnier et al., 2014] [Vidale et al., 2014].
The second level consists of both detection and location of the damage. Frequency variations might only reflect an overall change in the system properties, and this is often not sufficient to locate the origin of the perturbation within the structure. Damage detection methods have therefore been

developed based on mode-shape analysis. These methods are based on the mode-shape derivatives that give the position of the damage, and they include the mode flexibility method [Pandey and Biswas, 1994], the curvature flexibility method [Zhang and Aktan, 1995], and the mode-shape curvature (MSC) method [Pandey et al., 1991], or a combination of these methods. In actual buildings, the experimental assessment of mode shapes is not always accurate enough to detect and locate small variations, compared to the sensitivity of modal frequency analysis. The spatial resolution of local perturbations requires a sufficient number of modes, which is related to the spatial wavelengths of the higher-order mode shapes [Turek and Kuperman, 1997]. In addition, the participation of each mode in the total building response limits the accurate assessment of mode shapes using ambient vibrations. Moreover, the experimental assessment of mode shapes in actual buildings takes time, which is not always an option in a crisis management situation, and its accuracy is not always sufficient to detect and locate small variations.

The objective of the present study was to provide a comparison of damage identification algorithms for beam-type structures. Identification and location of specific damage in a beam-type structure is an important benchmark for post-earthquake assessment of the integrity of actual structures. Only four NDE algorithms were tested in this study, which were based on finite element simulation and experimental simulation at the laboratory scale, and were for different scenarios (e.g., single, multiple, position of the damage). Fan and Qiao [2010] have already compared the efficiency of NDE methods on modal-based numerical simulation. The present study differs in that the detection and location are performed through consideration of equivalent *in-situ* situations, and that it is oriented toward post-earthquake management; i.e., after extraction of the mode shapes and the frequencies of the structure using operative modal analysis methods applied to simulated and/or experimental ambient vibrations, and considering a limited and finite number of sensors and noisy signals. After presenting the experimental and numerical simulations developed for the one-dimensional (1-D) free-clamped bending beam, the mode-shape–based methods are described and their efficiencies are evaluated using the experimental and synthetic data.

2. Numerical and experimental simulation

2.1 Numerical simulation

The finite element model of the uniform free-clamped 1-D beam is discretised with n_b=200 finite elements of the same length δ (Fig. 1a). The Euler-Bernoulli beam theory is used to constitute the finite element matrices. The element has a constant moment of inertia *I*, modulus of elasticity *E*, density *ρ* and length *L*, and the shear deformation and rotatory inertia are neglected. The degree of freedom of the beam is therefore $n_{dof}=2(n_b+1)$, and the variable vector element of the j^{th} beam as defined by two nodes is $\{u^j\}=\{u_j \;\; \theta_j \;\; u_{j+1} \;\; \theta_{j+1}\}^T$, where *u* is the transverse displacement along the *y*-axis, and *θ* is the rotation around the *x*-axis of node *j*. Considering *E* and *I*, the elementary stiffness matrix at the j^{th} beam element of height *δ* is defined according to Humar [1990]:

$$K_{el}^{j} = \frac{EI^{j}}{\delta^{3}} \begin{bmatrix} 12 & 6\delta & -12 & 6\delta \\ & 4\delta^{2} & -6\delta & 2\delta^{2} \\ & & 12 & -6\delta \\ sym. & & & 4\delta^{2} \end{bmatrix} \tag{2.1}$$

The total stiffness matrix *K* is obtained by assembling the contribution of all of the j^{th} element stiffness matrices. The boundary conditions at $x=0$ correspond to $u_1=\theta_1=0$. The equation of the motion for a undamped multiple-degree-of-freedom structural system is represented as follows:

$$[M]\{\ddot{u}\} + [K]\{u\} = \{F(t)\} \tag{2.2}$$

where $\ddot{u}$ and u are the acceleration and displacement vectors, respectively, for the whole structure, and F is the external force vector. Under free vibrations, the natural frequencies ω and the mode shapes Φ of the system are obtained by solving the linearised eigenvalues problem:

$$[K] - \omega^2[M]\{\phi\} = 0 \tag{2.3}$$

where M is the global mass matrix that is obtained in the same way as the stiffness matrix K by correctly assembling the element mass matrices [Bathe, 1996]. The wave equation at time $t+\Delta t$ that governs the linear dynamic response of a complete element assembly is defined as:

$$M\{\ddot{u}^{t+\Delta t}\} + K\{u^{t+\Delta t}\} = \{F^{t+\Delta t}\} \tag{2.4}$$

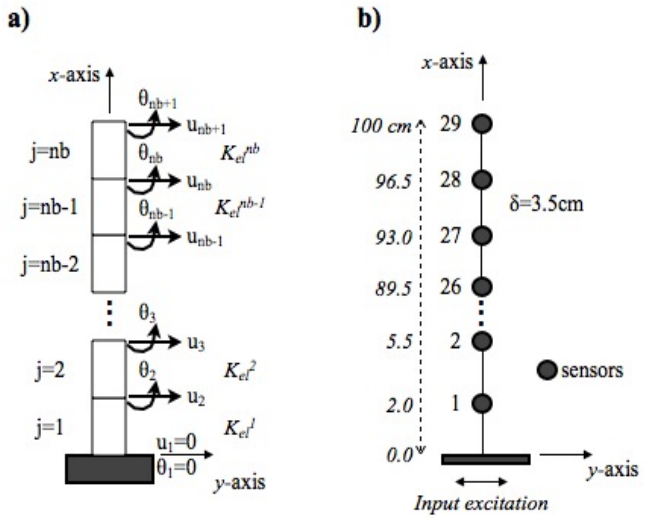

Figure 1: *a) Illustration of the finite element model of the 1-D beam discretised by j = 1,nb Euler-Bernouilli finite elements. Here, u_i is the transverse displacement, θ_i is the rotation of node i and K_{el}^j is the nb element stiffness matrix assembly used to obtain the total stiffness matrix K of Equation 2.1. b) Position of the nodes (sensors) where the vibration of the beam is computed.*

The displacements are integrated using the Newmark's numerical step-by-step scheme [Newmark, 1959] and the constant-average-acceleration method is used as follows:

$$\dot{u}^{t+\Delta t} = \dot{u}^t + \Delta t[(1-\gamma)\ddot{u}^t + \gamma\ddot{u}^{t+\Delta t}]$$

$$u^{t+\Delta t} = u^t + \dot{u}^t\Delta t + \frac{\Delta t^2}{2}[(1-2\beta)\ddot{u}^t + 2\beta\ddot{u}^{t+\Delta t}] \tag{2.5}$$

where γ and β are the parameters that define the method. The method is implicit, and stability is guaranteed for $2\beta \geq \gamma \geq 0.5$ [Bathe, 1996]. In our case, the trapezoidal rule is considered, i.e. β=0.25 and γ=0.5.

In this study, the characteristics of the 1-D bending beam are equivalent to the polymethyl methacrylate (Plexiglas) beam used for the experimental approach; i.e. height H = 1m, width W = 0.05 m, depth D = 0.01 m, Young's modulus E = 5.4 GPa, density ρ = 1165 kg/m^3 and inertial moment I = 4x10^{-9} m^4. The beam is discretized with 200 elements, with an element spacing δ = 0.5 cm (Fig. 1b). We consider a free-clamped boundary condition, anchored at the bottom ($x = 0$) and free at the end ($x = H$). At x = 0, low-amplitude white noise excitation is applied perpendicular to the beam axis. The noise is generated randomly using a normal distribution with a zero mean value and a standard deviation of 10^{-6}. At x = 0, the displacement varies arbitrarily with time, and its

rotation remains null. The noise signal propagates into the beam, and the time histories of the beam vibrations are computed at 29 nodes, from x = 2cm to x = 100cm (at 3.5 cm intervals). During the synthetic experiment, noise excitation was maintained for 300 s, and the sampling frequency was 5,000 Hz (Δt = 0.0002 s). The damage was modeled by reducing the Young's modulus (and then the stiffness *EI;* Eq. 2.1) according to the relation:

$$E^* = (1-a)\,E \qquad (2.6)$$

where E^* and E are the damaged and undamaged Young's moduli, respectively. Eleven scenarios (Tab. 1, 1-11) were tested, with single or multiple perturbations, different levels of severity (coefficient *a,* Eq. 2.6) and different positions of these perturbations along the beam (Tab. 1). Each scenario corresponded to one numerical experience with the perturbation at position A, B, C or D along the building height, and scenarios 9 to 11 corresponded to multiple perturbations applied simultaneously.

Table 1. *Values and positions of the stiffness variations along the building height. The values correspond to coefficient a in Equation 2.6.*

Damage position	**Perturbation**	**Perturbation position[a] (cm)**	**Stiffness reduction according to 11 scenarios**									
			S1	**S2**	**S3**	**S4**	**S5**	**S6**	**S7**	**S8**	**S9**	**S10**	**S11**
Undamaged	n.a.	n.a.	0										
A	Single	30.0-33.5		0.2	0.5	0.7	0.9				0.9	0.9	0.5
B	Single	61.5-65.0						0.9			0.9	0.7	0.7
C	Single	86.0-89.5							0.9		0.9	0.5	0.9
D	Extended	30.0-47.5								0.9			

[a], position of perturbation from the bottom (x = 0)

2.2 Analogous simulation in the laboratory

Equivalent analogous simulations were performed at the laboratory scale. The structure used in this study was a continuous poly(methyl methacrylate) beam, anchored at the bottom and free at the end (i.e., a free-clamped beam). Figure 2 shows the experimental set-up used to study the bending vibration in the *xy* plane (Figure 1). The data were acquired using 29 accelerometers that were powered by two conditioning amplifiers. The accelerometers were mono axial (Bruel and Kjaer, Type 4344) with a mass of 1.45 g and a frequency band of 1 Hz to 20 kHz. All of the sensors were oriented horizontally, on the widest face of the beam, to record the beam vibration in the y direction. The amplifiers were connected to a data acquisition unit via an RS232 port, which allowed certain acquisition parameters to be defined and controlled, such as the gain of each accelerometer. A maximum gain of 40 dB was selected to amplify the signal recorded by each sensor. The beam vibrations recorded by the accelerometers were transmitted directly to a computer by the data acquisition unit. The accelerometers were spread up the height of the beam at 3.5-cm intervals. An air jet that represents low amplitude white noise excitation continuously excited the beam. Several configurations were tested with the jet in different positions and orientations, and this configuration was as close as possible to the ambient noise of actual buildings. The data were collected as 10-s windows at a sampling frequency of 5,000 Hz (Figure 2). The transfer of these data to the acquisition unit took about 20 s, and consequently the experiment recording was not totally continuous. The perturbation was introduced by heating the continuous poly(methyl

methacrylate) beam locally at each of the positions A, B, and C, as indicated in Figure 2. Unlike the numerical model, the cases studied here were single damage scenarios with the perturbation applied at each position. The perturbation severity and length were not controlled.

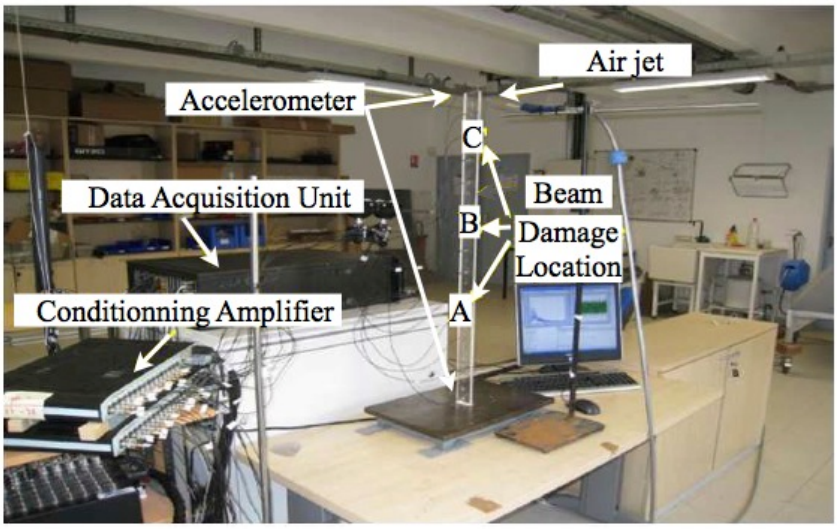

Figure 2. *The experimental set-up with the 29 accelerometers spread up the 1-m-long poly(methyl methacrylate) beam that was anchored to a metal plate. The accelerometers were equally spaced from top to bottom, and the beam was forced into vibration by an air jet applied at the free end of the beam. A, B and C indicate the locations of the perturbations produced by heating the poly(methyl methacrylate) beam*.

3. Methods for locating and detecting damage

In most cases, the detection of structural damage is based on comparisons of the building response before and after damage. As the ambient vibrations that are recorded in actual structures represent an efficient means for the extraction of modal parameters, mode-shape derivative methods were used in the present study.

3.1. Mode-shape curvature method

Pandey et al. [1991] used the change in the mode shape curvature (MSC) as an indicator of damage, with the assumption that that structural damage affects the structure stiffness matrix (*EI*) and causes changes in the MSC. According to elementary beam theory, the curvature at a location x along a beam is:

$$u''(x) = \frac{M(x)}{EI} \tag{3.7}$$

where *M(x)* is the bending moment at location *x*. Represented in the normal mode domain, the MSCs are derived using a central difference approximation, as follows:

$$\phi''_{i,j} = \frac{\phi_{i+1,j} - 2\phi_{i,j} + \phi_{i-1,j}}{\delta^2} \tag{3.8}$$

where $\Phi''_{i,j}$ is the modal curvature, *i* is the node number, *j* is the corresponding mode shape number, δ *is* the uniform length of discretisation elements (the distance between the nodes) and $\Phi_{i,j}$ *is* the normalised modal value for the i^{th} node (*P* nodes or position of sensor) in the j^{th} mode (*N* modes). The damage location was assessed by the largest absolute changes in the MSC, given by:

$$MSC_i = \sum_{j=1}^{N} \left| \phi''^{*}_{i,j} - \phi''_{i,j} \right| \tag{3.9}$$

where * is the damaged state, and *N* is the number of modes used. By plotting the MSC values along the beam at the *P* positions of the nodes, a maximum appears at the damaged element. Pandey et al. [1991] stated that the MSCs might also show some small peaks at different undamaged locations when higher modes are considered, which will introduce some false detections. They concluded that a small number of mode shapes must be used for damage identification.

3.2 Mode-shape curvature squared method

Ho and Ewins [2000] proposed the MSC squared (MSCS) method as an improved means for the location of damage with respect to the MSC. The MSCS is mathematically expressed as:

$$MSCS_i = \sum_{j=1}^{N} \left| \left(\phi_{i,j}''^{*}\right)^2 - \left(\phi_{i,j}''\right)^2 \right| \tag{3.10}$$

As with Pandey et al. [1991], Ho and Ewins [2000] stated that higher derivatives of mode shapes are more sensitive to damage and to errors in mode-shape measurements.

3.3 Change in flexibility method

Pandey and Biswas [1994] showed that the flexibility matrix of a structure *[F]* can be approximated using the unit-mass normalized modal data, as:

$$[F] \approx [\phi][\Omega]^{-1}[\phi]^T = \sum_{i=1}^{N} \frac{1}{\omega_i^2}\{\phi_i\}\{\phi_i\}^T \tag{3.11}$$

where Ω (=diag(ω^2_i)) is the modal stiffness matrix. Equation 3.11 can be extended to the damage flexibility matrix F^* considering the mode shapes Φ^* and the frequency ω^* of the damaged state. The change in flexibility (CIF) can be obtained from the difference between the respective matrices of *[F]* and *[F*]*, as:

$$[\Delta F] = [F^*] - [F] \tag{3.12}$$

3.4 Change in uniform-load surface curvature

Zhang and Aktan [1995] combined certain aspects of the MSC and CIF methods to develop the change in uniform-load surface curvature (ULS) method, which considers the flexibility matrix *[F]* as the translational displacement under a unit load at the jth degree-of-freedom. The curvature change at location *i* is evaluated as follows:

$$\Delta F_i'' = \sum_{i=1}^{N} |\{F_i''^{*}\} - \{F_i''\}| \tag{3.13}$$

where $F^{*\prime\prime}_i$ and F''_i are the second derivative functions of the flexibility matrix that correspond to the damaged and undamaged curvatures, respectively, of the uniform load surface at the i^{th} degree of freedom. The ULS is first evaluated for each unit load flexibility shape, and then it is summed. The ULS can be obtained using a central difference operator (Equation 3.8). Wu and Law [2004] applied the ULS method to plate structures for damage location and quantification also with truncated, incomplete, and noisy measurements.

3.5. Modal analysis

To extract the frequencies and mode shapes of the beam using simulated and experimental data, the frequency domain decomposition (FDD) technique that was developed by Brincker et al. [2001] was applied, because of its accuracy and simplicity. The FDD method is a nonparametric operational modal analysis, and no prior model is needed for the data processing. FDD is becoming a standard method among output-only techniques, as it has been used successfully in a number of studies and implemented in commercial software [Magalhaes et al., 2007] [Gentile et al., 2007] [Brinker et al., 2001] [ARTeMIS, 2008]. A detailed discussion and the theoretical background of the FDD method can be found in Brincker et al. (2001). FDD estimates the eigenvalues and

eigenvectors of the system (mode shapes and frequencies) by diagonalizing the power spectra density matrix; i.e., by computing the Fourier spectra of the cross-correlation matrix of simultaneous recordings made in the system. FDD has been widely used recently for output-only system identification for actual tall buildings, which has confirmed its reliability and effectiveness [Michel et al., 2008] [Michel et al., 2010]. For the present study, we estimated the spectral density matrices of the data and computed the singular value decomposition of the spectral density matrices. The data were processed according to the description provided in Michel et al. [2008] [2010] for actual buildings. For numerical analysis, the response of the model are applied without considering the signal-to-noise ratio; however, the accuracy of the frequency estimation classically depends on the signal-to-noise ratio but a low signal-to-noise ratio can be overcome by increasing the length of the time window used for modal analysis.

4. Results

4.1 Modal analysis of the numerical and experimental simulation

The first analysis of the beam response was obtained relatively easily by computing the Fourier spectrum (Fast Fourier Transform) at each accelerometer or node, which represents the classical peak-picking method. Figure 3 shows the Fourier amplitude variation along the beam according to numerical modeling and the experimental configuration. The theoretical behavior of a continuous beam is observed, with nodes and anti-nodes of the mode shapes. The frequency ratios of eigenfrequencies of the beam obtained in the experiments were f_2/f_1=6.3, f_3/f_1=18.4 and f_4/f_1=35.8, and from now on, we always assume bending beam behavior. As expected, the experimental mode shapes are noisier than the numerical ones, and only the first eight modes are clearly observed in the experimental modeling. The excitation used for the experimental simulation was applied at the top of the beam, assuming an equivalent white noise. Compared to the white noise spectra applied at the bottom of the numerical beam, experimental white noise is not a perfect assumption, introducing some variations in the mode shapes assessment.

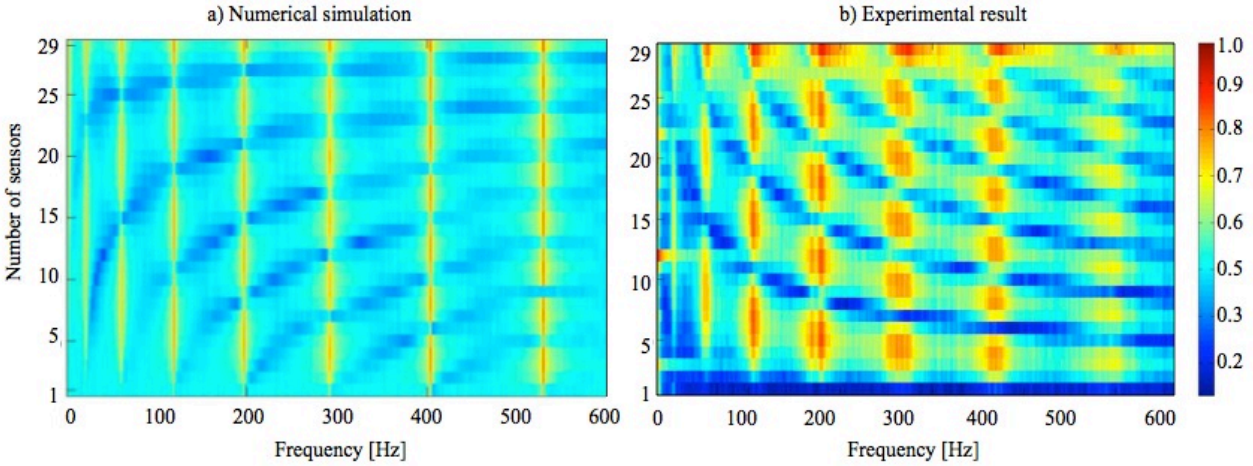

Figure 3. *Normalized amplitude of the Fourier spectra computed at the 29 sensors and representing the eight first shapes of the numerical simulation (a) and the experimental result along the undamaged beam (b). The color scale is representative of the normalized amplitude of the Fourier spectra at the top of the beam.*

The first singular values of the power spectra density matrix are shown in Figure 4, considering several of the damage scenarios reported in Table 1, and the associated mode shapes for the numerical simulation and experimental data. We obtained a clear assessment of the modes, in terms of frequencies and mode shapes. As expected, the numerical results are less noisy than the experimental data. For the experimental data, because of the nonperfect white noise spectra of the

air jet applied at the top of the beam (less white at lower frequencies), the shape of the first mode is not well represented and it was not considered in the subsequent experimental analysis. Furthermore, between the undamaged and damaged states, there was a shift in the frequencies, according to the severity of the stiffness reduction (Figure 4a). The modes do not all have the same sensitivity to damage, as the position of the stiffness reduction does not have the same effect, which depends on the positions of the mode-shape nodes and anti-nodes along the beam. Although the experimental data are noisier, we observe a shift in the frequencies of the first five modes, with this information integrated at the end for the location and detection of changes.

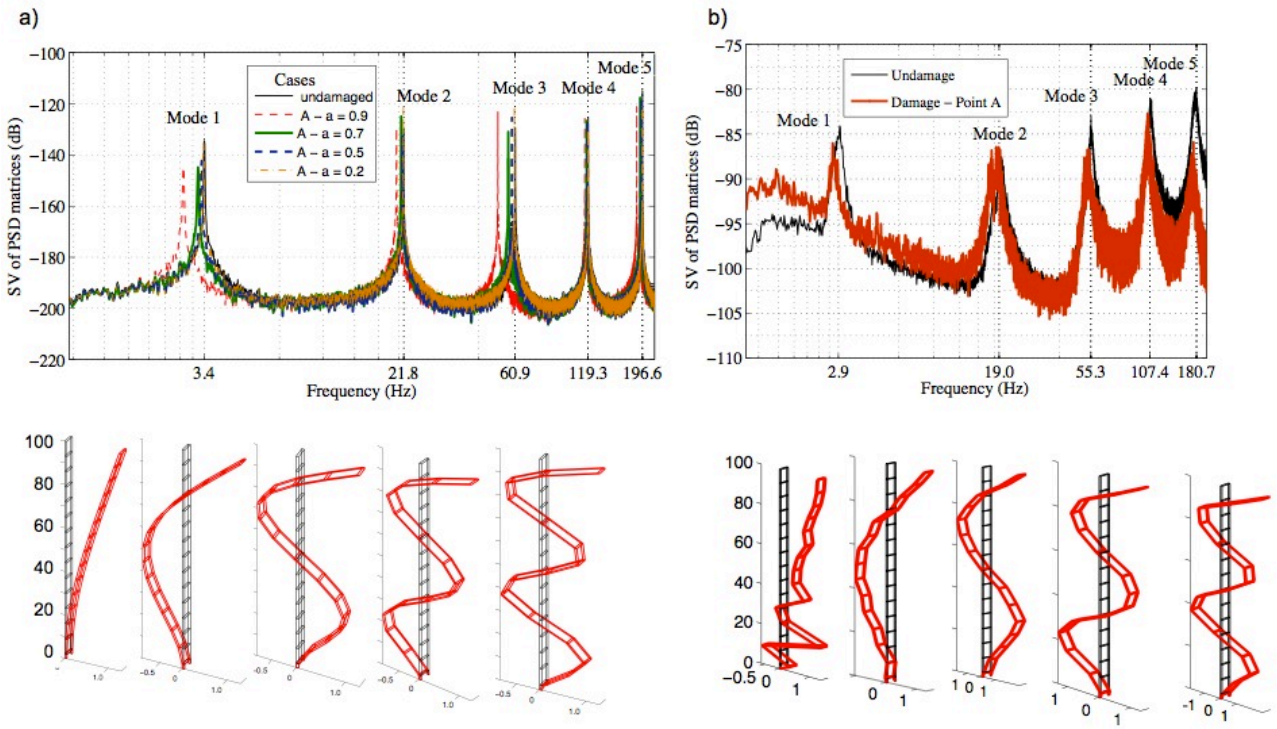

Figure 4. *First singular vectors obtained with the frequency domain decomposition method for the numerical (a) and experimental (b) approaches, and associated mode shapes that correspond to the first five modes. The singular vectors show the different scenarios for the damaged and undamaged beams, while the mode shapes are only for the undamaged beam.*

Table 2 presents a comparison of the eigenfrequencies obtained by theoretical analysis using the solutions of the eigenvalue problems (Equation 2.3), the time analysis of the simulated ambient vibrations, and the experimental results. This comparison confirms the good match with the frequencies obtained by the modeling of the first eight bending modes with the equivalent experimental data. The frequencies ranged from *ca*. 3 Hz to 550 Hz, and these values were considered for the damage detection. There are differences between the numerical and experimental approaches, which are essentially related to the uncontrolled boundary conditions at the bottom of the experimental beam, and the mass added to the system by the sensors. The model is very simple and the aim of the paper is not to fit the experimental model. Goodness-of-fit was not the main aim of this study, but it might be increased by tuning of the numerical model. The comparison between numerical and experimental data was planned for comparing the efficiency of the damage localisation methods and we have focused on this point rather than on the fit to the model.

Table 2. *Frequencies of the initial undamaged beam through the solution of the eigenvalue problems, and application of the FFD method to the numerical simulation and to the experimental data*.

Mode	Frequency - Hz		
	Theoretical	Numerical	Experimental
1	3.47	3.47	2.90
2	21.79	21.79	18.99
3	61.00	61.02	55.33
4	119.52	119.59	107.37
5	197.51	197.69	180.73
6	292.93	295.31	272.52
7	411.76	412.46	372.94
8	547.94	549.14	500.24

4.2 Location and detection using modal based methods applied to the experiment based on numerical data

In this section, the four NDE methods defined previously (MSS, MSCS, CIF and ULS) were applied to the numerical vibrations of the beam using the first eight mode shapes and frequencies extracted using the FDD method, before and after each scenario listed in Table 2. As the local methods tested here were used for damage location, the damage assurance criterion of the estimated C_D was defined using the following formulation:

$$C_D = \frac{\left|\sum_{k=1}^{N}(L_R)_k(L_E)_k\right|^2}{\sum_{k=1}^{N}(L_R)_k^2 \sum_{k=1}^{N}(L_E)_k^2} \tag{3.15}$$

where L_R and L_E are the curves that represent the position of the normalized damage along the beam in the reference model and the numerical simulation, respectively. The reference model is defined as 0 for an undamaged section, and 1 for a damaged section, as shown Figure 5. A C_D close to 1.0 indicates that the NDE method was effective; a C_D significantly lower than 1.0 implies that the method did not accurately locate the damage or that there were several peaks that corresponded to false alarms with the NDE methods. This quality criterion was applied to each scenario (Table 1), to test the position and nature (i.e., single, multiple, extended) of the damage. As an example, Figure 5 shows the reference position of the damage model and the positions estimated by the ULSC and MSC methods for the S5 damage scenario (position A, a = 0.9; see Table 1).

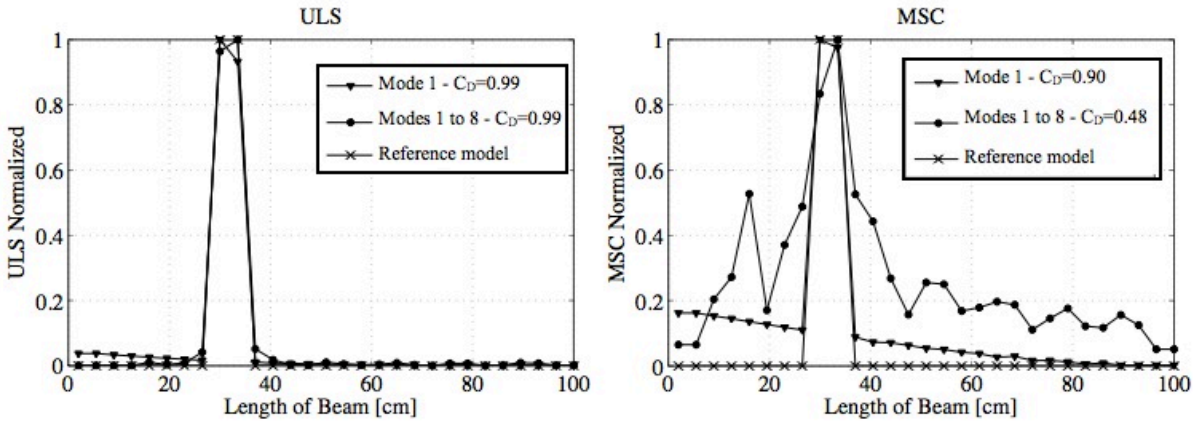

Figure 5. *Examples of the normalized criteria for damage location along the beam using the ULS and MSC methods for scenario S5 (position A, a = 0.9; see Table 1). The corresponding C_D assurance criteria are given in the keys, considering only one or eight modes. The reference model represents the position of the target damage along the beam (Equation (3.15), L_R), defined as 0 for undamaged sections, and 1 for damaged sections.*`

Following Equation 3.15, the C_D values for the ULS are 0.99 for the one or eight modes considered, and the C_D values for the MSC method are 0.90 and 0.48 for the one or eight modes, respectively. Even if the damage location was accurately detected by the MSC, false alarms were generated when eight modes were considered, which implies limited efficiency of the method for the estimation of the damage position in practice.

Figure 6 gives a summary of the results for each scenario for the four NDE methods. We show the variations in C_D according to the number of modes used, considering single or multiple damage locations; i.e., scenarios S5 to S9 (see Table 1). The CIF appears to be the worst method, as it does not detect the damage position for any of the scenarios. For all of the scenarios, C_D is below 0.8, with the best efficiency being for S9 (multiple damage). This method is not discussed further in the text.

For the MSC and MSCS, their location is more efficient when a small number of modes was considered, and C_D decreases for single damage when more modes were considered. As previously reported by Pandey et al. [1991] for the MSC method, higher order modes introduce bias into the assessment, due to the inadequate accuracy of the mode shapes for a limited number of nodes. To reduce the probability of false detections, these two methods (i.e., MSC, MSCS) need the first two mode shapes to locate the damage with good accuracy. Depending on the nature of the damage, variations are observed. The best resolution is observed for single damage at position A, B or C (scenarios S5, S6, S7). For a small number of modes, variations of C_D are observed with the MSC, which depended on the position of the perturbation along the beam. This is less pronounced for the MSCS method for perturbations located at A or B, but the damage position at the free end of the beam is less defined (i.e., for position C, scenario S7). In the presence of major damage at A (scenario S8) or multiple damage (scenario S9), C_D reaches a maximum value with at least four modes, but with a value below 0.8. The results thus depend on the nature of the damage, and the large fluctuation of C_D reflects the poor efficiency of these methods if the damage type is not known in advance.

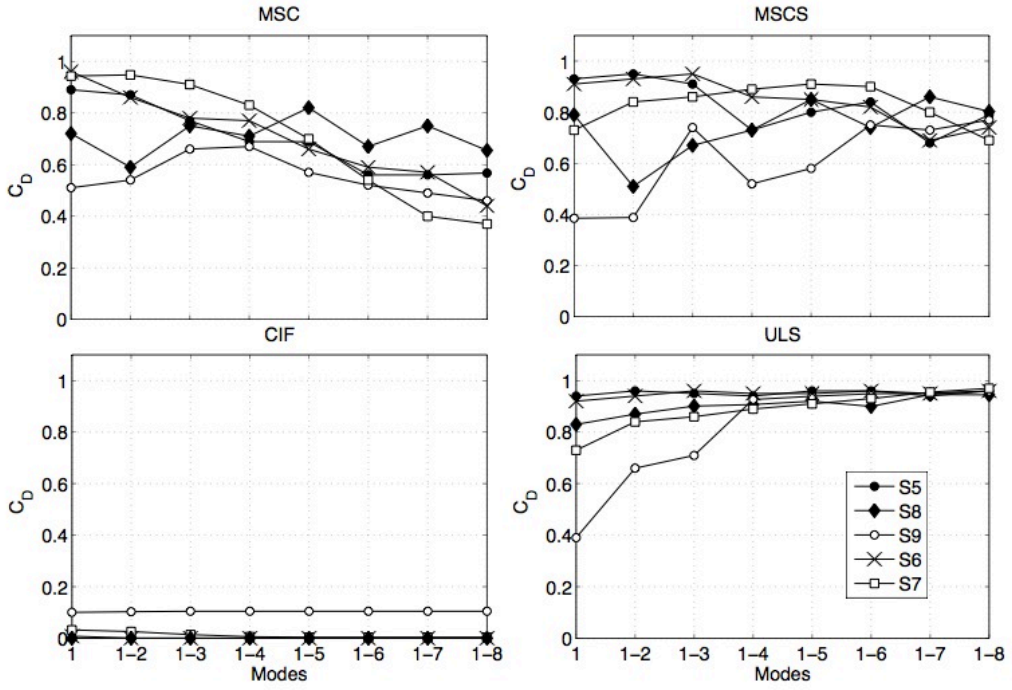

Figure 6. *Comparison of the assurance criteria of location C_D obtained with the MSC, MSCS, CIF and ULS NDE methods for scenarios S5 to S9, including single and multiple damage, and*

considering between one and eight modes extracted by FDD from the synthetic ambient vibration recordings.

Compared with other methods, the ULS is certainly the most efficient method for locating perturbations, with stable and constant values of C_D close to 1.0 even with a limited number of modes, which is the case for *in-situ* building experiments. With at least 4 modes, the positions of single, multiple or major damage are well defined, with these modes usually obtained for actual tall buildings with ambient vibrations. The efficiency of the ULS method depends on the position of the damage along the beam. Regardless of the number of modes, the damage location near the clamped boundary (scenario S5) is better solved than when the perturbation is located at the free end (scenario S7). This reflects the model of the beam considered in this study, i.e., the bending beam, as the variation in the stiffness at the end of the beam has less influence on the shape of the modes. Other beam models (shear beam or Timoshenko) should be tested in the future. For major and multiple damage (scenarios S8, S9), the ULS method is the most effective, with C_D over 0.8. For major damage, the ULS efficiency is not highly dependent on the number of modes, and C_D increases slightly. For multiple damage (scenario S9), the ULS fails to locate the damage considering only the first modes and the optimum is reached with the first four modes, which is relevant to field experiments on tall buildings. For scenarios S5 to S9, the location accuracy was not improved (C_D remains constant) by introducing more modes into the process (over five), which suggests that only the first five modes were required to locate the damage, regardless of the scenario. In terms of practical efficiency, the ULS is not sensitive to the nature of the damage, and it can be applied without *a-priori* information of the damage position.
For single and multiple damage at different levels of severity (i.e., varying *a*), the ULS method was applied with the first five modes. Figure 7 shows the damage location for scenarios S2 to S5 (single damage at point A, with different levels of severity; see Table 1) and for scenarios S10 and S11 (multiple damage at points A, B and C, with different levels of severity; see Table 1). Only the ULS method is considered, and the first five modes extracted from simulated ambient vibrations are integrated into the process.

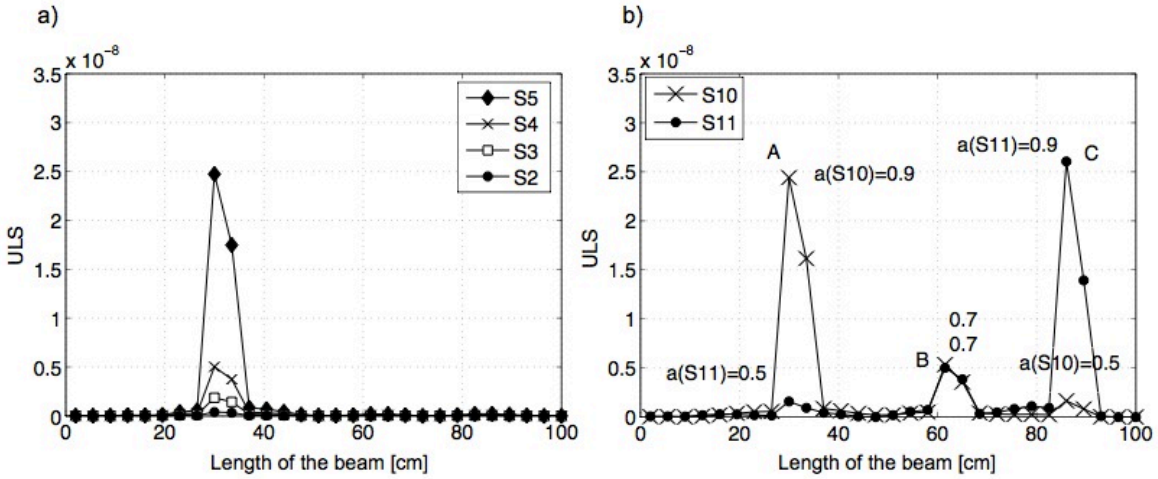

Figure 7. *Effect of the severity of damage (for a from 0.2 to 0.9) on the efficiency of the ULS method, considering a single damage position (scenarios S2 to S5) (a), and multiple damage positions at A, B and C (scenarios S10 and S11) (b). Only the first five modes were used in the process.*

The absolute amplitude of the damage was not the main purpose of this test, and will not be further discussed here. For single damage (Figure 7a), the relative amplitude of the damage is well represented by the ULS method, as well as its location. The amplitude of ULS at point A increases

from the lowest (a = 0.2) to the highest (a = 0.9) values of stiffness reduction. It is also important to note that the increase is not linear with severity, as the absolute amplitudes of the ULS are not directly related to the stiffness reduction. For the lowest level of severity (a = 0.2), the ULS at point A is higher than the ULS for the undamaged sections along the beam. In all cases, the correlation coefficients C_D are 0.98, with this coefficient related only to the good location of the damage, without considering the amplitude. For multiple damage (Figure 7b), C_D ranges from 0.98 (scenario S11) to 0.97 (scenario S10), according to the position of the greatest damage relative to the free extremity of the beam. As shown before, ULS locates the multiple damage perfectly along the beam, without introducing any false alarms. Moreover, the relative amplitude of the amount of damage (coefficient a, Equation (2.6)) is respected considering the least severe to the most severe damage. For example, the magnitude of the multiple damage is respected when the strongest damage (a = 0.9) is located at A or C, as well as for the smallest amplitude (a = 0.5). These data highlight the efficiency of the ULS method for accomplishing levels I (detection) and II (detection and location) of the health monitoring strategy. Level III is not completely accomplished since absolute severity is not assessed. Nevertheless, considering the relative damage assessment as a key factor in the safety assessment of actual buildings after earthquakes, ULS provides some key information for relative damage assessment.

4.3 Experimental results

In the following, we aimed to determine the efficiency of the ULS method for the location of some small damage along the beam in an equivalent-to-real experiment; i.e., with noisy modes and frequencies. Two experiments were carried out. In the first experimental set-up (E1), the poly(methyl methacrylate) beam was heated at three positions near the clamped boundary: at A (30-33.5 cm from the bottom), at the middle position B (61.5-65 cm from the bottom) and at the free end for position C (86-89.5 cm from the bottom). The heat flow was applied to the beam 2 h, 4 h, and 6 h after the beginning of the experiment, at positions A, B and C, respectively, and the duration of the heating was 30 s in each case. The second experiment (E2) consisted of increasing the duration of the heating period at position D, at 40.5 cm from the bottom. Forty-five minutes after the beginning of the experiment, the heat flow was applied for 12 min. In both experiments, 29 sensors were used to record the vibrations of the beam excited by an air jet that was applied at the top (Figure 2).

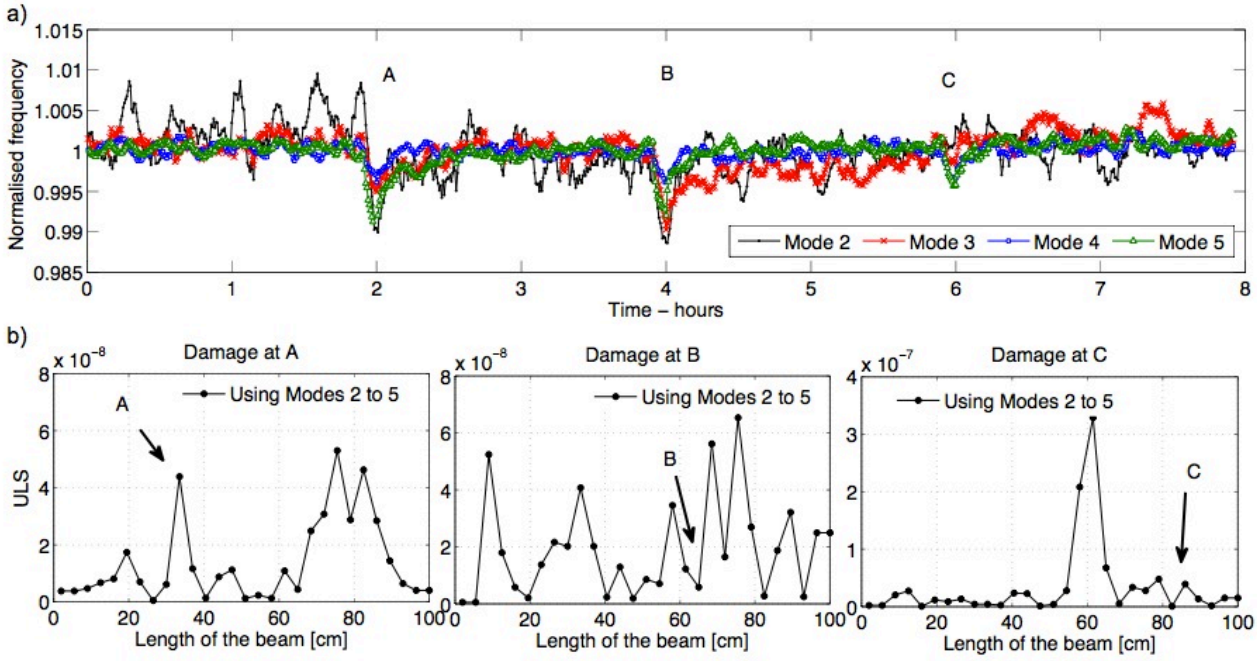

Figure 8. *Experimental results (E1) of heating at points A, B and C of the poly(methyl methacrylate) beam. (a) Variation of the normalized frequency of modes 2 to 5. (b) Location of the damage with the ULS considering modes 2 to 5 for damage at A, B, and C.*

Figure 8 shows the results of experiment E1. The variations in the normalized frequency for modes 2 to 5 are shown in Figure 8a, as extracted from the free end recordings using the random decrement technique. This method enables efficient monitoring of frequency variations using continuous recordings for actual buildings [Mikael et al., 2013] or in laboratory-scale tests [Roux et al., 2014]. It consists of stacking short time-windows of ambient vibrations that have the same triggering conditions, to obtain the impulse response of the system. The frequency is then estimated directly from the impulse response. The description of this method is beyond the scope of this study, and so we refer the reader to Roux et al. [2014] for the processing details. In Figure 8a, there was softening of the beam with damage located at A and B and with smaller amplitude at C. As expected, the frequency variation is much noisier than for the numerical study and depends on the position of the damage, as the modes do not all react in the same manner. Figure 8b shows the ULS results considering the damage at A, B and C successively. The frequencies and mode shapes are obtained using FDD applied to 30-s windows selected 1 h after the beginning of the experiment, and the equivalent window at the time of the damaged state. There is very poor efficiency for the ULS method: the damage at B and C is not located, and false alarms are generated (C_D less than 0.2, considering the reference position of the damage equivalent to position D; see Table 1). This is also the case for the damage at A, even if the location is identified ($C_D = 0.42$). One condition for an accurate estimation of the mode shapes using FDD is the application of the Welch method [Michel et al., 2008; 2010] to reduce noise in the estimated power spectra by averaging overlapping time windows. In the present case, the heating period was short (30 s) which limited the number of windows selected for the averaging process.

The second experiment E2 was conducted by increasing the duration of the heating period to improve the mode-shape assessment with FDD. Figure 9 shows the results of experiment E2. The variation in the normalized frequency for modes 2 to 5 is shown in Figure 9a, as extracted from the free-end recordings using the random decrement technique. There is improved and less noisy evaluation of the damage, with the magnitude of the softening of the frequencies directly related to the duration of the heating period. As noted previously for experiment E1, for each modal frequency, the magnitude of the variation is influenced by the position of the perturbation along the beam, in relation to the nodes and anti-nodes of each mode shape. This affects the efficiency of each mode for the location of the damaged position, as shown in Figure 9b. As for experiment E1, the frequencies and mode shapes are obtained using the FDD method applied to a window selected before and during the heating; i.e., a 12-min window. Using the ULS method and considering only one mode, the location is more or less identified, with some false alarms generated for the mode that is the least sensitive to the perturbation (C_D close to 0.95 for modes 2 and 4, and less than 0.55 for modes 3 and 5). Finally, the ULS method is applied to modes 2 to 5 (Figure 9c), and as shown for the numerical simulation, the method succeeds perfectly in location of the damage ($C_D = 0.95$). The 12-min-long heating period means that the mode-shape resolution using FDD is improved and the variation of the stiffness is better identified.

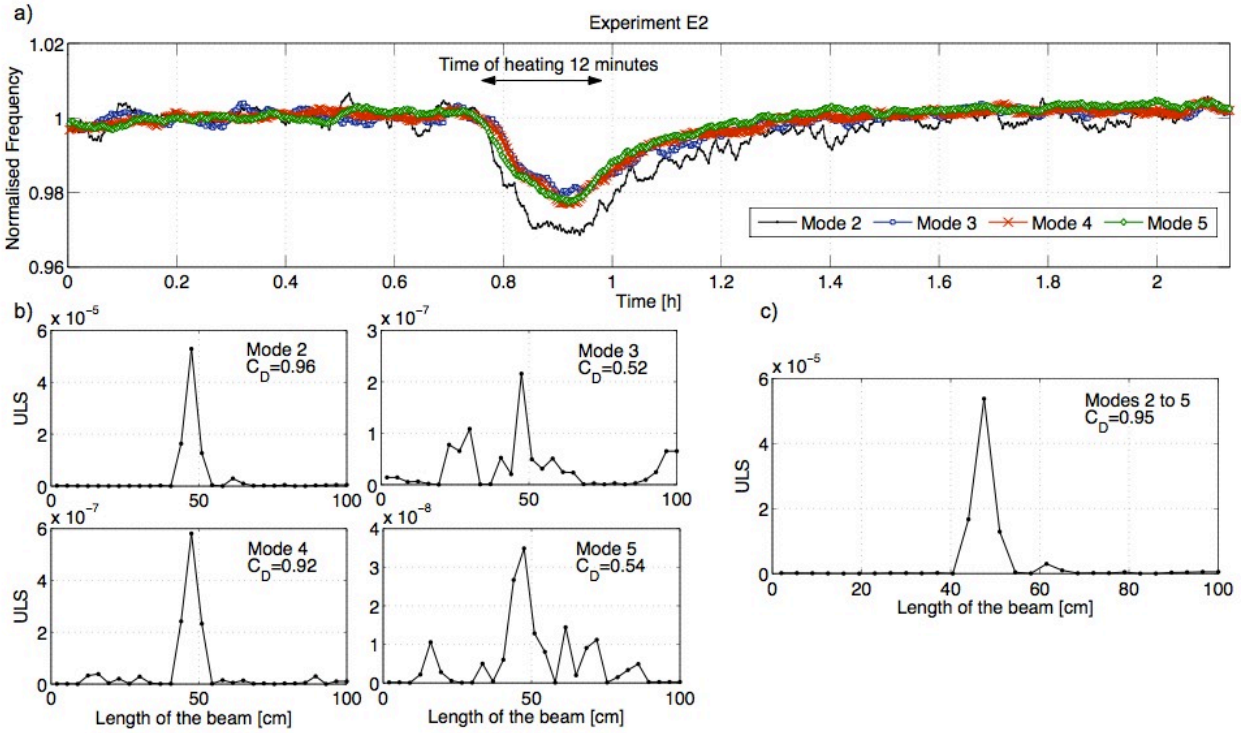

Figure 9. *Experimental results (E9) with heating at 40.5 cm from the clamped boundary of the beam. (a) Variation in the normalized frequency of modes 2 to 5. (b) Location of the damage with ULS considering a single mode (modes 2 to 5). (c) As for (b), considering modes 2 to 5 together.*

6 Conclusions

This study has discussed the non-invasive evaluation of damage via changes in the dynamic modal response of a structure. The main goal was to evaluate four NDE methods that were designed to detect and locate damage in a continuous beam, which represents a real structure. The basic idea is that the modification of the stiffness characteristics of the system can alter its dynamic response. A beam-structure was modeled, and perturbations were induced by reducing the Young's modulus in local or extended zones along the beam. Compared with previous studies [Fan and Qiao, 2010], the effectiveness and robustness of the methods are tested in a configuration that is equivalent to that used experimentally for post-earthquake building assessment, i.e. applying operative modal analysis methods to ambient vibration recordings done along the beam (building) height.

In the present study, numerical analysis with low-amplitude excitation was used to test the efficiency of the NDE methods under different configurations (i.e., single, extended, multiple damage). Ambient vibrations were simulated and operative modal analysis was used to provide mode shapes and frequencies. The results show that the correlation coefficient C_D is highest for the ULS method, and that this method is more efficient than the MSC, MSCS and CIF methods, regardless of the nature and position of the damage. No false alarms are generated, and without *a-priori* information on the damage localization, we can obtain a reliable description of the damage, in terms of detection and location, and also relative severity. From a practical point of view, with only five modes, the ULS method identifies the location of the damage, and these modes can be obtained easily in actual tall buildings using ambient vibrations. This conclusion is confirmed by experiments carried out in the laboratory with a poly(methyl methacrylate) beam. Even with noisy vibrations, the ULS locates the site of a single damage occurrence.

One drawback is the extensive deployment of instrumentation needed to estimate the mode-shape fluctuations for mode-shape curvature methods. Roux et al. [2014] proposed an innovative approach based on perturbation theory using frequency variations; this approach requires only one sensor that records ambient vibrations at the top of the building. As for the ULS, this method might only be successful in simple structures. This is the case for most tall buildings, the behavior of which is well represented by continuous beam theory and is more sensitive to boundary conditions. While the perturbation method is accurate for weak perturbation, the ULS is more efficient for major damage. The combination of the frequency variation and mode-shape curvature methods might improve the efficiency of damage location in actual buildings, as shown by comparing MSC or MSCS methods to ULS method. Different beam models, actual complex structures, and sensitivity to noise measurements will be tested in the future, to further define the performance of the ULS method with field data.

Acknowledgments
The authors would like to thank the "Région Rhône Alpes" for financial support for this project. This work also received financial support from DREAL (Direction Régionale de l'Environnement, de l'Aménagement et du Logement) and FEDER within the framework of the RiskNat project in the ALCOTRA (2007-2013) program.

8. References

Bathe, K.J. [1996] *Finite Element Procedures*, Prentice-Hall, ISBN-81-203-1075-6, 1037p.

Brincker, R., Zhang, L., and Andersen, P. [2001] "Modal identification of output-only systems using frequency domain decomposition," *Smart Materials and Structures* **10(3)**, 441.

Doebling, S.W., Farrar, C.R., and Goodman, R. [1997] "Effects of measurement statistics on the detection of damage in the Alamosa Canyon bridge," in Proceedings of the 15th International Modal Analysis Conference, Orlando, FL, USA.

Fan, W., and Qiao, P. [2010] "Vibration-based damage identification methods: a review and compartive study," *Structural Health Monitoring* **10**, 8383-110.

Farrar, C.R., and Worden, K. [2007] "An introduction to structural health monitoring", Phil. Trans. R. Soc. London **365,** 303–315.

Gentile, C., Gallino, N., Lourenço, P., Oliveira, D., and Portela, A. [2007] "Ambient vibration-based investigation of the Victory arch bridge", *Proc, 5th Int. Conference on Arch Bridges (ARCH'07)*, 63-70.

Ho, Y., and Ewins, D. [2000] "On the structural damage identification with mode shapes", *Proceedings of the European COST F3 conference on system identification and structural health monitoring*, pp. 677-686.

Humar, J.L. [1990] *Dynamics of Structures*. Prentice-Hall, ISBN 0-13-222068-7, 780p.

Magalhães, F., Caetano, E., and Cunha, A. [2007] "Challenges in the application of stochastic modal identification methods to a cable-stayed bridge," *Journal of Bridge Engineering* **12(6)**, 746-754.

Michel, C., Guéguen, P., El Arem, S., Mazars, J., and Kotronis, P. [2010] "Full Scale Dynamic response of a RC building under weak seismic motions using earthquake recordings, ambient vibrations and modelling," *Earthq. Engng and Struct. Dyn*. **39**, 419–441, doi 10.1002/eqe.948.

Michel, C., Guéguen, P., and Bard, P.-Y. [2008] "Dynamic parameters of structures extracted from ambient vibration measurements: An aid for the seismic vulnerability assessment of existing buildings in moderate seismic hazard regions", *Soil Dynamics and Earthquake Engineering* **28(8)**, 593-604. doi:10.1016/j.soildyn.2007.10.002

Mikael, A., Guéguen, P., Bard, P.-Y., Roux, P., and Langlais, M. [2013] "Long-term frequency and damping wandering in buildings analysed using the Random Decrement Technique (RDT)", *Bull seism. Soc. Am.* **103(1)**, 236-246, doi 10.1785/0120120048

Newmark, N.M. [1959] “A method of computational for structural dynamics”, *ASCE Journal of Engineering Mechanics Division* **85**, 67–94.

Pandey, A.K., Biswas, M., and Samman, M.M. [1991] “Damage detection from changes in curvature mode shapes,” *Journal of Sound and Vibration* **145(2)**, 321-332. DOI: 10.1016/0022-460X(91)90595-B.

Pandey, A.K., and Biswas, M. [1994] “Damage detection in structures using changes in flexibility”, *Journal of Sound and Vibration* **169(1)**, 3–7. DOI: 10.1006/jsvi.1994.1002,

Régnier, J., Michel, C., Bertrand, E., and Guéguen, P. [2013] “Contribution of ambient vibration recordings (free-field and buildings) for post-seismic analysis : the case of the Mw 7.3 Martinique (French lesser Antilles) earthquake, November 29, 2007”, *Soil Dynamics and Earthquake Engineering* **50**, 162-167. doi 10.1016/j.soildyn.2013.03.007

Roux, P., Guéguen, P., Baillet, L., and Hamze, A. [2014] “Structural-change localization and monitoring through perturbation-based inverse problem,” *Journal of the Acoustical Society of America* **136**, 2586. doi: 10.1121/1.4897403.

Rytter, A. [1993] “Vibrational based inspection of civil engineering sructures”. PhD thesis, Aalborg University.

Salawu, O. S. [1997] “Detection of structural damage through changes in frequency: A review”, *Engineering Structures* **19(9)**, 718–723.

Turek, G, and Kuperman, W.A. [1997] “Applications of matched-field processing to structural vibration problems”, *Journal of the Acoustis Sociey of America* **101(3)**, 1430–1440.

Vidal, F., Navarro, M., Aranda, C., and Enomoto, T. [2014] “Changes in dynamic characteristics of Lorca RC buildings from pre- and post-earthquake ambient vibration data,” *Bulletin of Earthquake Engineering* **12(5)**, 2095-2110

Wu, D., and Law, S. [2004] "Damage localization in plate structures from uniform load surface curvature," *Journal of Sound and Vibration* **276(1)**, 227-244.

Zhang, Z., and Aktan, A.E. [1995] “The damage indices for constructed facilities,” *Proc. IMAC 13* 1995; Nashville, 1520–1529.

Valutazione numerica e sperimentale delle prestazioni di quattro metodi non distruttivi di identificazione del danno in situazioni analoghe ad analisi di danno post-terremoto.

Philippe Guéguen*, Alaa Hamze*,Laurent Baillet*, Philippe Roux*

*ISTerre, CNRS/IFSTTAR, Grenoble Alpes university, BP 53, 38041 Grenoble cedex9, France,
Corresponding Author: Philippe Guéguen - philippe.gueguen@ujf-grenoble.fr

SOMMARIO – questo studio considera diversi metodi di riconoscimento e localizzazione di variazioni delle caratteristiche di risposta di una trave inflessa. Lo scenario scelto e' confrontabile con una situazione in-situ post terremoto. La stima dello stato di danneggiamento di un edificio e' un aspetto cruciale della fase di gestione dell'emergenza. Le condizioni degli edifici possono essere verificate attraverso l'utilizzo di metodi di analisi modali basati su vibrazioni ambientali. In questo studio quattro metodi sono stati valutati per la localizzazione di una condizione di danneggiamento. Valori di frequenze e forme modali di una trave sono stati calcolati attraverso un modello a elementi finiti e successivamente ottenuti per un modello di trave in Plexiglas incastrata alla base e libera alla sommita'. Il confronto tra diversi approcci indica il metodo " uniform load surface curvature" come il piu efficiente ed accurato nella localizzazione del danno, qualunque sia la sua natura (semplice, multiplo, in diverse posizioni etc.). I dati sperimentali sottolineano inoltre la necessita' di accurate identificazioni dellle forme modali altrimenti penalizzanti la localizzazione di danneggiamenti transienti.

Parole Chiave: danno, localizzazione. metodi modali, sperimentale, numerico